ACS OMEGA

Open Access

http://pubs.acs.org/journal/acsodf

Article

Higher-Order Structural Analysis of a Transparent and Flexible High Thermal Conductive Liquid Crystalline Elastomer Sheet and Its Composite

Yoshitaka Takezawa,* Naoki Furukawa, Senguttuvan Nachimuthu, Risheng Zhou, and Amir Torbati

Cite This: *ACS Omega* 2024, 9, 20839−20848

Read Online

ACCESS | Metrics & More | Article Recommendations | Supporting Information

ABSTRACT: Transparency, flexibility, and high thermal conductivity are trade-offs. Specifically, we have investigated a cross-linked acrylic liquid crystal elastomer (LCE) that exhibits both transparency and flexibility while maintaining a high level of thermal conductivity. The transparent monodomain LCE sheet was achieved through a process of stretching an initially opaque polydomain sheet to 80% elongation and subsequently subjecting it to photocuring. The thermal conductivity in the stretching direction (x) of the monodomain LCE sheet was found to be 1.8 times higher than that of the prestretched polydomain sheet, consistent with findings from previous studies. However, in the orthogonal direction (y) to the stretching (x) direction, the thermal conductivity exhibited an even higher value, being 1.7 times greater than in the x-direction, with a value of 3.0 W/(m·K). This unique observation prompted us to conduct further investigation through higher-order structural analysis of these LCE sheets using 2D wide-angle X-ray scattering (WAXS) analysis. In the transparent sheet, the LCE molecules were aligned in the sheet in the stretching x-direction (monodomain structure) for the out-of-plane direction. However, in the in-plane x-direction, the molecular plane spacing exhibited random orientation at a period of 0.45 nm. In contrast, within the y-direction of the inner layer, the molecular plane spacing exhibited a uniaxial horizontal orientation at the same period length as in the x-direction. The heat energy entering into the y-direction once spreads to the x-direction, but it was considered that the reason for the higher thermal conductivity to the y-direction would be forming covalent bonds that function as new heat transmission paths, in the direction intersecting to the x-direction during photocuring. Therefore, we concluded that the synergistic effect of the high level of the ordered inner structure and covalent bonding structure due to cross-linking in the y-direction contributes to its higher thermal conductivity compared to that in the x-direction, which exhibits a random in-plane structure. Additionally, we have fabricated an LCE composite sheet filled with 75 vol % of alumina particles using a polydomain-type LCE as the base material. The composite sheet exhibits remarkable thermal conductivity in the thickness direction, measuring at 9.8 W/(m·K), while maintaining a flexibility characterized by an elastic modulus of 70 MPa. This thermal conductivity surpasses that of a nonmesogenic acrylic composite sheet with identical alumina particle filling, which measured at 3.9 W/(m·K), more than twice as much. The presence of the mesogen skeleton has been demonstrated to enhance heat transfer, even within soft composites, by facilitating the formation of an ordered structure.

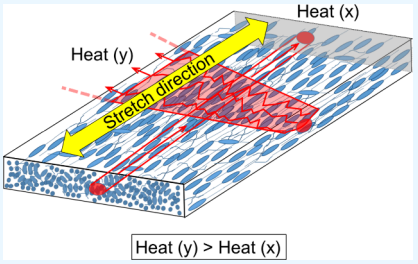

1. INTRODUCTION

As electronic devices become more sophisticated and compact, the heat generation density in circuits is increasing. Consequently, there is an increasing demand for enhanced heat dissipation, especially for electric insulating materials.[1−4] Although polymers are excellent electric insulating materials, they are basically adiabatic and do not conduct heat effectively. This is because, unlike metals, which have free electrons that facilitate heat conduction, in insulating polymers, phonons dominate thermal conduction.[5] Polymers are broadly classified into thermoplastic and thermosetting polymers, and it is known that the thermal conductivity of thermoplastic polymers increases when they are stretched.[6−14] Recently, it has been reported that the thermal conductivity of polyethylene fiber, a thermoplastic polymer, was increased to 104 W/(m·K), which is equivalent to that of metal, by stretching it to the utmost limit.[15,16] In contrast, thermosetting polymers that form a three-dimensional network structure, such as epoxy resin, which is an essential material for electronic circuits, cannot be stretched or otherwise oriented like thermoplastic polymers, making it difficult to significantly improve their thermal conductivity. Therefore, to reduce phonon scattering and achieve high thermal conductivity, it is effective to form a highly ordered higher-order structure inside the polymer by self-alignment of the mesogen backbone,[4,17−38] and then to

Received: November 30, 2023
Revised: April 24, 2024
Accepted: April 26, 2024
Published: May 4, 2024

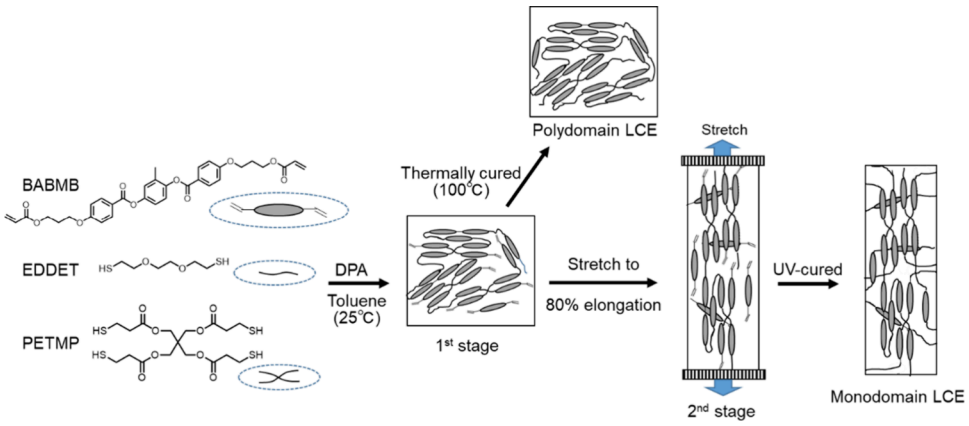

Figure 1. Schematic fabrication process of two types of LCE polydomain and monodomain sheets.

design molecules that increase the cross-linking density by selecting a curing agent.[2] Recently, a research study utilized a mesogen epoxy resin film alone, without the addition of a thermally conductive ceramic filler, and achieved a thermal conductivity of 10 W/(m·K).[39] Although thermoplastic polymers exhibit a significant decrease in the thermal conductivity above Tg, thermosetting polymers experience a minor decrease in thermal conductivity. This is attributed to the preserved cross-linked orientation order in thermosetting polymers even when above Tg.[1,2]

However, transparency, flexibility, and high thermal conductivity are in a trade-off relationship within polymers. Thus far, a polymer that successfully embodies all three characteristics simultaneously has not yet been developed. Several papers had reported transparent polymer films with high thermal conductivity, but not enough transparency properties.[40,41] The introduction of a mesogen skeleton is effective in increasing thermal conductivity, but its high orientation and birefringence anisotropy result in a rigid and opaque structure.[2,18,35,36,39] Recently, a new liquid crystalline acrylic elastomer (LCE) sheet with transparency, flexibility, and impact strength resistance has been published in papers.[42−44] In this paper, monodomain and polydomain liquid crystal elastomers (LCEs), as well as LCE composites, are fabricated, and their thermal conductivities are measured. The study aims to investigate the relationship between higher-order structural analysis and thermal conductivity by utilizing XRD. The fabrication process of the monodomain LCE involves two stages. First, the LCE polydomain is achieved by employing Michael addition of polyeher thiols and multifunctional thiols to an acrylic monomer containing mesogens (1st stage). Subsequently, the material undergoes stretching and photo curing to transition into the monodomain state (2nd stage). Additionally, a flexible composite sheet of polydomain LCE with a high alumina filler content was fabricated without the stretching process. Subsequently, its thermal conductivity was evaluated.

2. EXPERIMENTAL SECTION

2.1. Preparation of LCE Polydomain, Monodomain, and Composite Sheets. LCE polydomain and monodomain sheets were fabricated in accordance with methods previously published,[42,43] and the schematic fabrication process is shown in Figure 1. For the LCE synthesis described here, 1,4-bis[4-(3-acryloyloxypropyloxy)benzoyloxy]-2-methylbenzene (BABMB: M.W. 588 g/mol) with 99% purity was purchased from Synthon Chemicals (Germany). Pentaerythritol tetrakis-(3-mercaptopropionate) (PETMP: M.W. 488 g/mol), 2,2-(ethylenedioxy)diethanethiol (EDDET: M.W. 182 g/mol), dipropylamine (DPA: M.W. 101 g/mol), and 2-hydroxy-4′-(2-hydroxyethoxy)-2-methylpropiophenone) (HHMP: M.W. 224 g/mol) were purchased from Sigma-Aldrich. The LCE material is made using a chemical composition (BABMB/EDDET/PETMP= 7/6/1 (mol ratio)), with the addition of toluene to facilitate the Michael addition reaction. Once the solution returned to room temperature (25 °C), 1 mol % DPA was added for the first-stage polydomain LCE polymerization as depicted in Figure 1. The polydomain LCE sheets were made by coating the solution on a PET film with a PTFE spacer under vacuum, subsequently postcured at 100 °C. For the monodomain LCE sheets, 1 mol % HHMP photoinitiator was added to first-stage material; the mixture was coated on a PET film with a PTFE spacer. After vacuuming to remove the solvent at room temperature, the precured LCE sheet was peeled from the PET film. Next, mechanical stretching was applied to the LCE sheet until it reached 80% elongation, as depicted in Figure 1 (2nd stage). In this study, the stretching condition was standardized at 80% elongation to ensure stability and prevent breakage, resulting in final thicknesses of 300 and 600 μm. After stretching, the width of the LCE sheet is reduced to approximately 70%, while the thickness is reduced to around 80%. Next, the LCE sheet is exposed to a 365 nm UV light source at an intensity of 10 mW/cm^2 for 10 min by holding a UV lamp approximately 150 mm from the sheet. The resulting cured sheet for evaluation measures 300 and 600 μm in thickness.

The LCE alumina composite sheet was fabricated following the procedure outlined in Figure S1. The LCE alumina varnish is made using the above LCE chemical composition (BABMB/EDDET/PETMP = 7/6/1 (mol ratio)), with the inclusion of toluene to aid the Michael addition reaction. The mixture of alumina powder (Advanced Alumina AA series; AA18 (mean diameter: 20 μm): AA3 (3.5 μm): AA04 (0.47 μm) = 66:24:10 (weight ratio)) purchased from Sumitomo Chemical was added. Since the alumina particle size has a distribution and the bulk density varies, the amount of alumina prepared for compositing is controlled by the weight ratio. Given the density of alumina and LCE are 3.98 and 1.25 g/cm^3, respectively, the weight ratio of LCE:alumina = 9.5:90.5 is equivalent to a volume ratio of LCE:alumina = 25:75. The LCE and alumina mixture varnish is mixed by a planetary centrifugal mixer (3 cycles for 5 min at 2000 rpm) at room

https://doi.org/10.1021/acsomega.3c09550
ACS Omega 2024, 9, 20839−20848

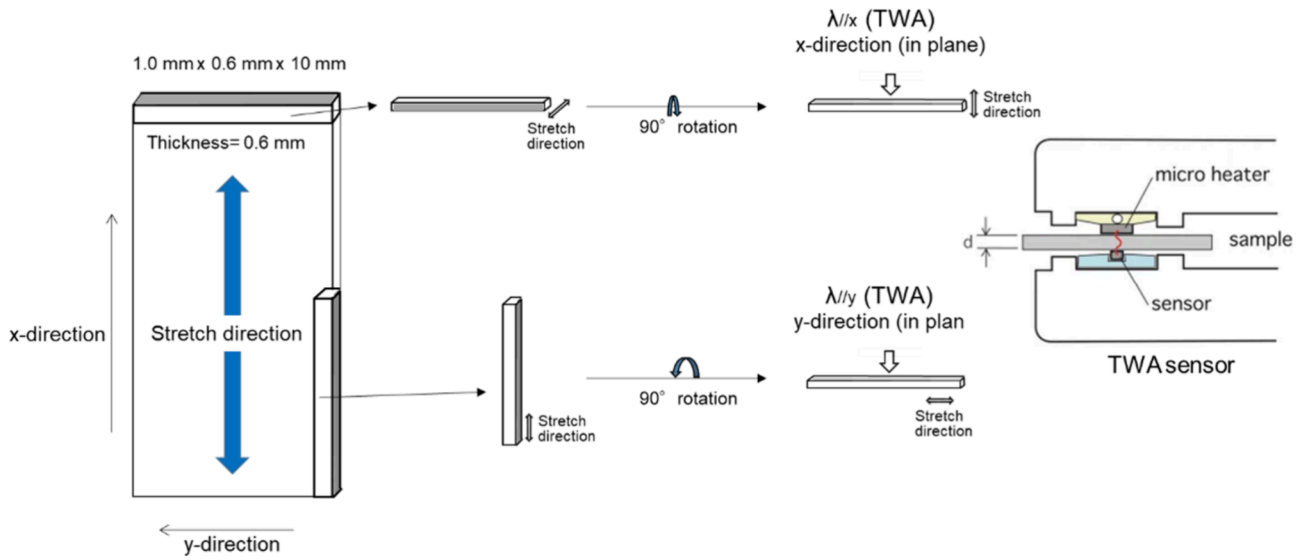

Figure 2. Processing method of LCE sheets used for measuring thermal diffusivities of each in-plane direction by the TWA method.

temperature, and toluene is added in minimal amounts necessary to facilitate the mixing of the alumina powder. Finally, 1 mol % DPA relative to the total chemicals amount (excluding alumina) was added, and the mixture was mixed by a planetary centrifugal mixer (1 cycle for 5 min at 2000 rpm). This compound varnish is injected into a mold using a PTFE spacer and release PET film as shown in Figure S1; subsequently, the compound is vacuum degassed at room temperature for 30 min and vacuum pressed for 30 min at 100 °C under 2 MPa to cure.

As a reference base resin, nonmesogenic multifunctional acrylic elastomer was used. For the reference base resin synthesis described here, *n*-butyl acrylate (BA: M.W. 128 g/mol) was purchased from Mitsubishi Chemical Co., trimethylplpropane triacrylate (TMPA: M.W. 296 g/mol) was purchased from Daicel-Allnex Ltd., 2-hydroxyethyl acrylate (HEA: M.W. 116 g/mol) was purchased from Nippon Shokubai Co. Ltd., and *t*-butyl peroxy-2-ethylhexanoate (PBO: M.W. 216 g/mol) as a polymerization initiator was purchased from the NOF corporation. Using the above chemical composition (BA/TMPA/HEA = 12/3/1 (mol ratio)), and incorporating the same alumina powder mixture as the LCE composite, a solution is prepared. Finally, 0.3 mol % PBO relative to the total chemical amount is added and thoroughly mixed.

2.2. Thermal Conductivity Measurement Method. The thermal conductivity (λ) of the LCE films was calculated as

$$\lambda = \alpha \times \rho \times C_p \quad (1)$$

where α, ρ, and C_p express the thermal diffusivity, density, and specific heat capacity of the LCE films, respectively. The thermal diffusivities of the LCE films were measured by temperature wave analysis (TWA)[45−47] using an apparatus (ai-Phase Mobile M3type1) based on ISO 22007. The configuration of the TWA apparatus and its features and principles are described in Figure S2. The ρ and C_p values were measured by the electronic hydrometer MDS-3000 (Alfa Mirage Co., Ltd.) and DSC 250 (TA Instrument), respectively.

The thermal diffusivity α of the LCE sheet was measured by cutting small pieces of the sheet against the thickness and in-plane direction as illustrated in Figure 2. The LCE monodomain sheets were measured for two directions: the stretch direction (x) and the orthogonal direction (y).

2.3. Higher-Order Structure Analysis Method. The higher-order structure of the obtained sheets was measured by transmission wide-angle X-ray scattering (WAXS) using the Rigaku SmartLab X-ray diffractometer and by transmission 2D-WAXS using the HyPix-3000 detector, which can measure two-dimensional images. The radiation source was CuKα radiation (λ = 0.15418 nm). It was used at 40 kV and 30 mA output. The diameter of the collimator was 0.1 mm. The camera length was 65 mm, and integrated measuring time was 120 min each. Using the Rigaku 2D Data Processing software "2DP", the 2θ diagram was described from the 2D data corrected for the scattering by the air atmosphere.

Polarized interference images of LCE polydomain and monodomain sheets were also qualitatively observed under crossed Nicols spectroscopy using a Nikon ECLIPSE LV100POL polarized optical microscope (POM).

2.4. Measurement of Elastic Modulus. The elongation at break and tensile modulus of the cured material were measured at 25 °C using a tensile tester (Autograph EZ-TEST EZ-S manufactured by Shimadzu Corporation). In the measurements, cured materials of dimensions 0.5 mm (thickness) × 5 mm (width) × 30 mm (length) were used. These samples were measured under the conditions of a 20 mm distance between chucks and a tensile speed of 5 mm/min. The elastic modulus is determined by the following equation based on the values of strain specified at two points.

$$E = (\sigma_2 - \sigma_1)/(\varepsilon_2 - \varepsilon_1) \quad (2)$$

where E expresses the elastic modulus (MPa), σ_1 expresses the stress (MPa) at strain ε_1 = 0.0005 (0.05%), and σ_2 expresses the stress (MPa) at strain ε_2 = 0.0025 (0.25%).

3. RESULTS AND DISCUSSIONS

3.1. LCE Polydomain and Monodomain Sheets. Figure 3 displays the appearance of the fabricated polydomain and monodomain LCE sheets, each with a thickness of 300 μm. The monodomain sheet exhibits transparency in the visible region. The transmittance spectrum of each LCE sheet was

https://doi.org/10.1021/acsomega.3c09550
ACS Omega 2024, 9, 20839−20848

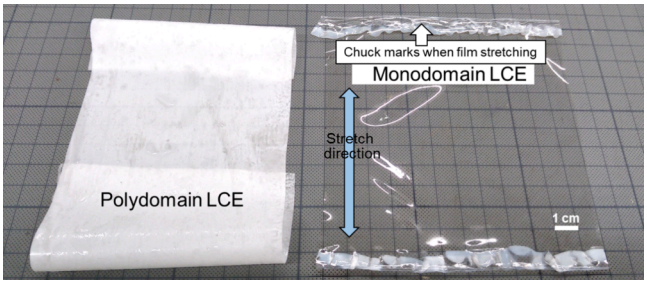

Figure 3. Appearance of the opaque polydomain and transparent monodomain LCE sheets (thickness = 300 μm).

measured using a Hitachi UV−vis−NIR Spectrophotometer (U-4000), as depicted in Figure S2.

First, the planar orientation of the LCE polydomain and monodomain sheet birefringence was qualitatively confirmed by rotating the stage under a crossed Nicols using a polarizing microscope (POM). The results are shown in Figure 4. For polydomain sheets, the brightness of the interference image did not change when the stage was rotated, whereas for monodomain sheets, the bright and dark fields repeated every 45° when the stage was rotated, indicating that the sheets were uniaxially oriented in the stretching direction within the plane.

Measurements of the in-plane thermal conductivity of LCE sheets were performed on 600 μm thick sheets. This choice was made due to the sensor size of the TWA apparatus, which is 0.25 × 0.5 mm (as illustrated in Figure S1). Table 1 shows the measurement results of thermal conductivities of each LCE sheets. The orientation of the thermal conductivity measurements is denoted by ∥ for in-plane and ⊥ for the out-of-plane (thickness) direction. The thermal conductivity of 0.35 W/(m·K) in the out-of-plane (thickness) direction for the polydomain LCE sheet is approximately three times higher than that of the monodomain LCE or reference acrylic elastomer sheet. It is hypothesized that the increase in the thermal conductivity of the polydomain LCE is attributed to the formation of an ordered structure facilitated by the presence of mesogens. In contrast, for the in-plane direction, both sheets exhibited thermal conductivities more than three times higher than those observed in the thickness direction. The reason for this phenomenon is assumed that the in-plane orientation would be formed by the effect of the hydrophobic surface of the PET film and the surface tension on the surface in contact with air. This is the typical characteristic of thermal conductivity anisotropy of polymer films; the longer molecular chains lie down randomly in the in-plane direction, as a result, facilitating heat transfer along the direction of the molecular chains rather than between molecules.[4,14,38,39,48−50]

In particular, the in-plane directional thermal conductivities of LCEs were over 1 W/(m·K), surpassing the in-plane thermal conductivity of polyimide (0.7−2.1 W/(m·K)).[4,38,50] The in-plane thermal conductivity of the monodomain was 1.8 W/(m·K) in the x-direction and 3.0 W/(m·K) in the y-direction, demonstrating very high values not seen in transparent and flexible polymers. In general, the thermal conductivity of polymer films increases in the direction of stretching and decreases tremendously in the thickness direction, as has been reported for PE and acrylic resins in many cases.[7−17] For this LCE, the thermal conductivity increased in the stretch direction as above and was even 1.7 times higher in the in-plane y-direction, which is orthogonal to the stretch direction. This unique phenomenon prompted the study of higher-order structural analysis for these LCE sheets by using X-ray diffraction (XRD) analysis.

Figure 5 shows the results of transmission 2D-WAXS measurements of LCE polydomain and monodomain sheets to the out-of-plane (thickness) direction. In the polydomain sheet (a), the intermolecular periodic structure (about 0.45 nm) around 2θ = 20° is isotropic and circularly scattered; although in the monodomain sheet (b), the intermolecular periodic structure around 2θ = 20° is strongly scattered in parallel to the LCE sheet stretching direction.

Focusing on the small angle region, a 2θ peak was observed at 2.7° (d = 3.25 nm) of polydomain sheet, but no peak existed for the monodomain sheet. Here, the molecular length of BABMB calculated from the linear distance between atoms in the MMFF94s force field using the structure optimization program Conflex is shown in Figure 6. The 2θ = 2.7° (d = 3.25 nm) value in Figure 5 is close to the molecular length of the BABMB.

Although the intensity of this peak is weak, it could be attributed to the periodic structure of the BABMB molecule. As shown in the schematic diagram in Figure 5, it is hypothsized that several mesogens would be periodically aligned in all directions, and the alkyl chains (EDDET, PETMP) are connected to BABMB in a random structure.

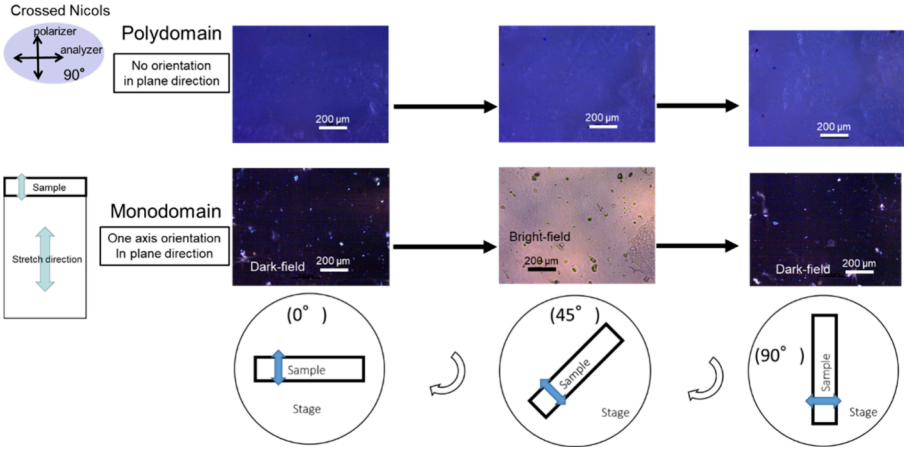

Figure 4. Observation of the orientation state of monodomain and polydomain sheets using a polarizing optical microscope (POM).

https://doi.org/10.1021/acsomega.3c09550
ACS Omega 2024, 9, 20839−20848

Table 1. Thermal Conductivities and Elastic Modulus for LCE Monodomain, Polydomain, and Reference Nonmesogenic Multifunctional Acrylic Elastomer Sheets (Thickness = 600 μm)

material	monodomain LCE		polydomain LCE		reference	
direction	∥ (in plane)	⊥ (out of plane)	∥ (in plane)	⊥ (out of plane)	∥ (in plane)	⊥ (out of plane)
thermal conductivity [W/(m·K)]	(1) *x*-direction: 1.8 ± 0.15 (2) *y*-direction: 3.0 ± 0.17	0.13 ± 0.02	1.0 ± 0.13	0.35 ± 0.04	0.30 ± 0.03	0.10 ± 0.02
density [g/cm3]	1.25 ± 0.01		1.25 ± 0.01		1.06 ± 0.01	
specific heat capacity [J/(g·K)]	1.20 ± 0.02		1.20 ± 0.02		1.93 ± 0.02	
elastic modulus [MPa]	0.15 ± 0.02		0.11 ± 0.01		0.05 ± 0.02	

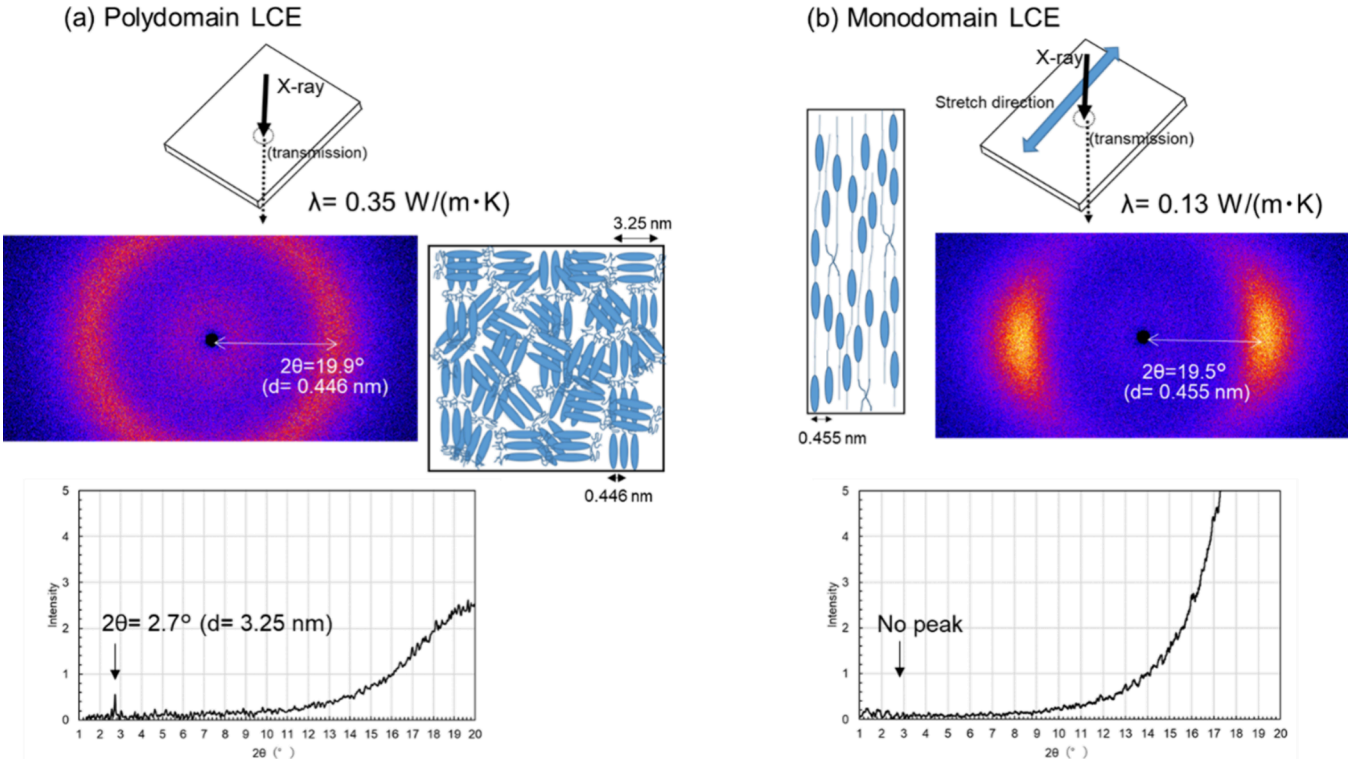

Figure 5. Higher-order structural analysis for (a) polydomain LCE and (b) monodomain LCE sheets, using transmission 2D-WAXS (out-of-plane direction) (thickness= 600 μm).

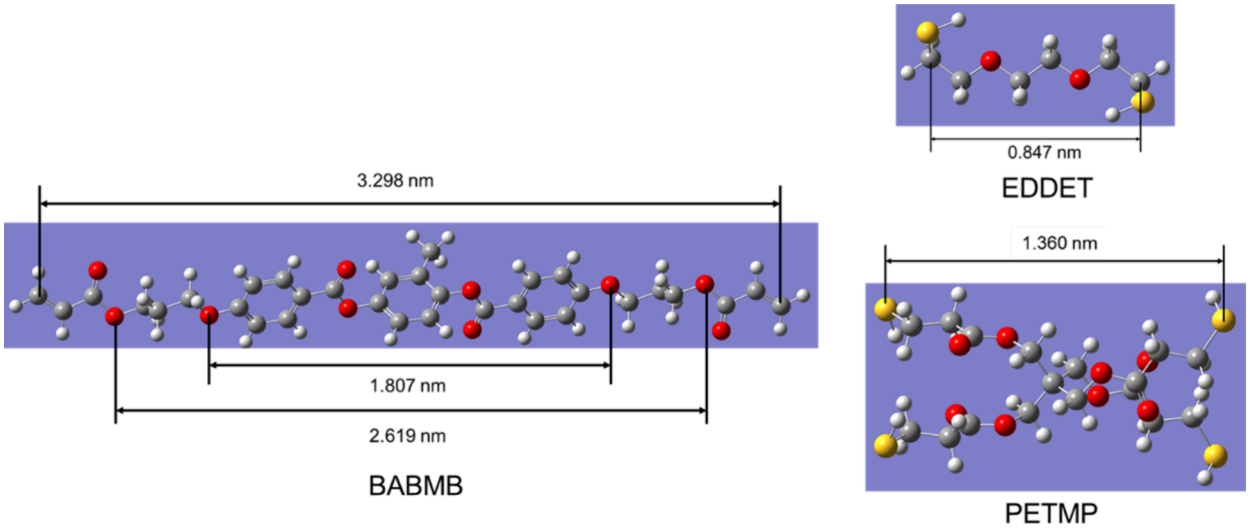

Figure 6. Molecular lengths of BABMB, EDDET, and PETMP calculated from linear distances between atoms in the MMFF94s force field using the "Conflex" program.

https://doi.org/10.1021/acsomega.3c09550
ACS Omega 2024, 9, 20839−20848

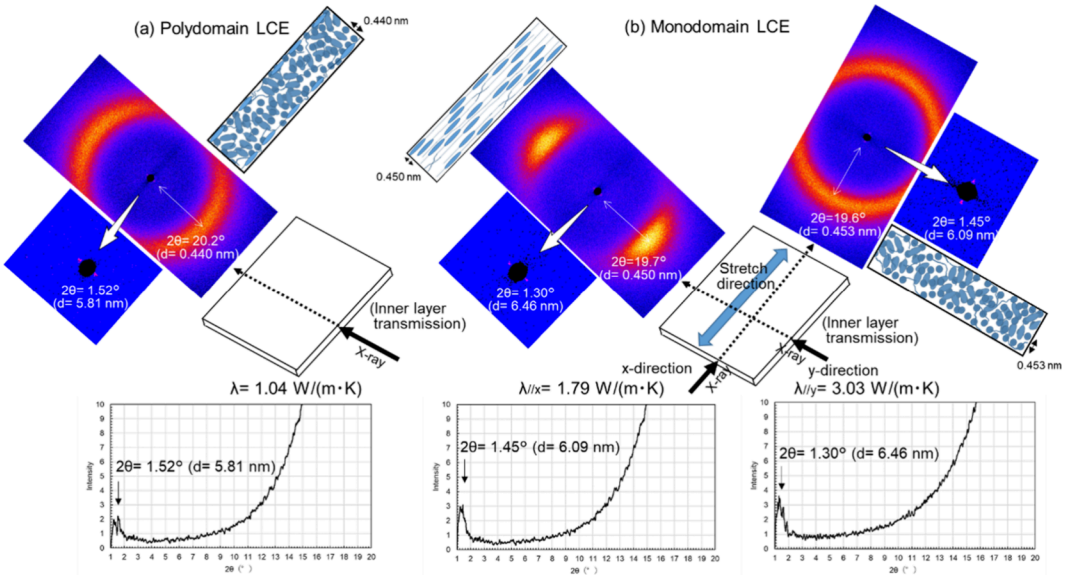

Figure 7. Higher-order structural analysis for (a) polydomain LCE and (b) monodomain LCE sheets, using transmission 2D-WAXS (in-plane direction) (thickness= 600 μm).

Next, the results of 2D-WAXS transmission measurements on the inner layer of LCE sheets were conducted and shown in Figure 7 and Figure S4. No directional differences were observed in the polydomain sheets in Figure S4; the circular diffraction scatter image, which exhibits almost isotropic characteristics but with a slight orientation toward the in-plane direction, was observed in the 2D-WAXS. However, significant differences in higher-order structure were observed between the *x*- and *y*-directions in the monodomain LCE sheets, as depicted in Figure 7b. Specifically, the intermolecular periodic structure (about 0.45 nm) around 2θ = 20° in the inner layer of the orthogonal *y*-direction to the stretching direction was strongly in-plane oriented in parallel to the stretching direction of the sheet. The characteristic four-point pattern to cybotactic nematics with stronger ordering[51−53] was not observed. In contrast, for the *x*-direction, a circular diffraction scattering image was observed in the 2D-WAXS image, suggesting that the intermolecular periodic structure is isotropic. No peak was observed at 2θ = 2.7° (d = 3.25 nm) for all LCE sheets, indicating no periodic structure of the BABMB molecule would exist in the inner layer.

Focusing on the small angle region, a weak but sharp scattering were observed in the vicinity of 2θ from 1.3° to 1.5° for all the sheets. Although the *d*-spacing is around 6 nm, which is nearly equivalent to two molecules of BABMB, the scattering direction is in the thickness direction of the LCE sheet. Additionally, the intensity is very weak compared to that of around 2θ = 20°; therefore, it is considered that there is little contribution to the thermal conductivity properties.

As shown in Figure 8, the slight difference in the periodic structure between the intermolecular planes at the wide-angle region (around 2θ = 20°) had little effect on the thermal conductivity. The width and thickness of the LCE sheet after stretching are macroscopically reduced to around 70 and 80%, respectively; however, the *d*-spacing is not changed nanoscopically. Therefore, it is considered that the reason for the higher thermal conductivity in the *y*-direction is due to the formation of covalent bonds that act as new heat transfer pathways in the direction intersecting with the *x*-direction during photo curing.

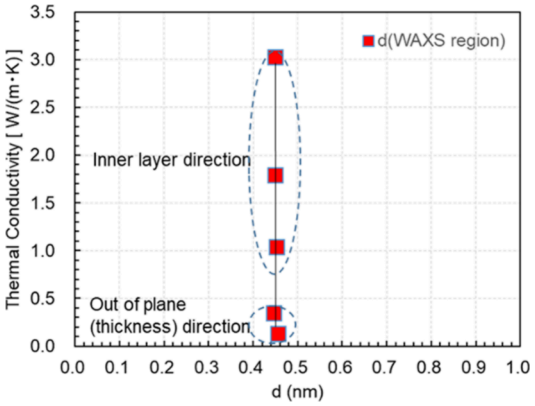

Figure 8. Relation between *d*-spacing values obtained from XRD analysis and their thermal conductivities (λ) measured by the TWA method (thickness= 600 μm).

Consequently, we concluded that the heat energy entering into the *y*-direction once spreads to the *x*-direction, but the synergistic effect of the high level of ordered inner structure and the covalent bonding structure due to cross-linking in the *y*-direction contributes to its higher thermal conductivity compared to that in the *x*-direction, which exhibits a random in-plane structure.

3.2. LCE Alumina Composite Sheet. Polydomain LCE, while soft and opaque, possesses high thermal conductivity in the thickness direction, so it might be applied to thermal interface materials (TIM) if it is made into a composite. Therefore, we aimed to fabricate the LCE alumina composite sheet for this purpose. Figure 9 illustrates (a) appearance of the obtained cured LCE alumina composite sheet with an alumina filler content of 75 vol % and a thickness of 300 μm, (b) a photo of the composite sheet wrapped around and adhered to a 6 mm diameter aluminum pipe demonstrating flexibility, and (c) confirmation of alumina filler dispersibility using POM (under crossed Nicols). As depicted in Figure 9b, the cured LCE alumina composite sheets have flexibility even with a 75 vol % alumina filler. The elastic modulus is approximately 70

https://doi.org/10.1021/acsomega.3c09550
ACS Omega 2024, 9, 20839−20848

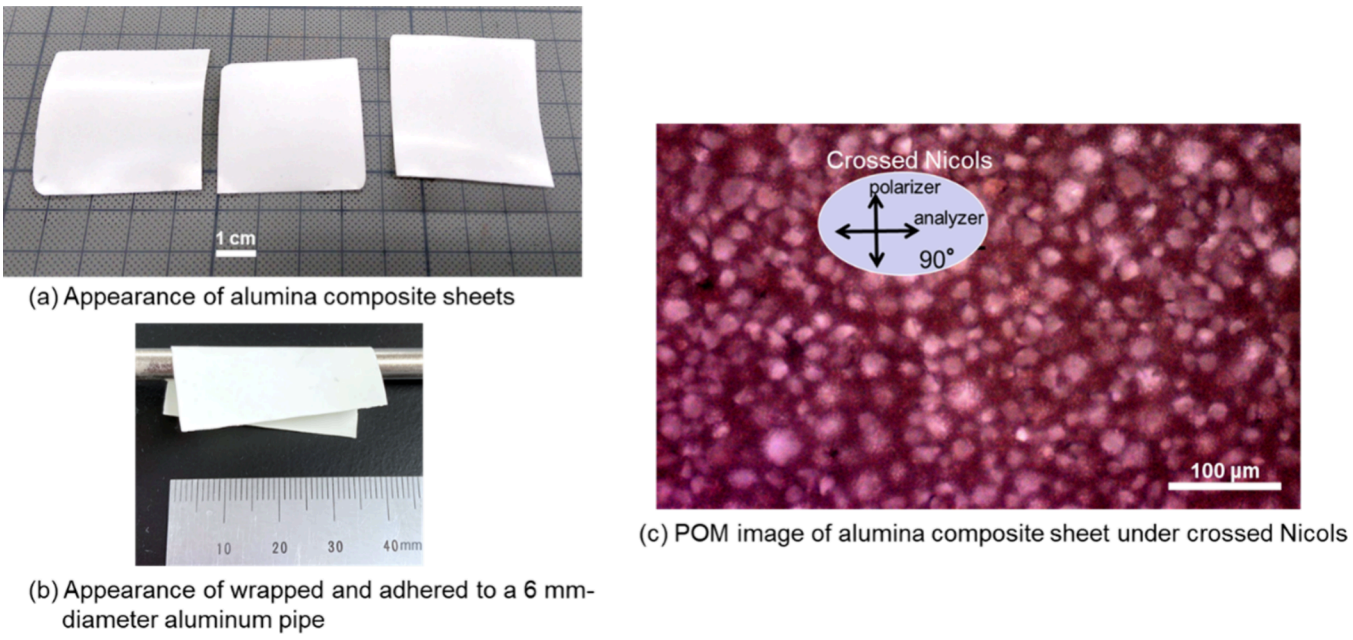

Figure 9. Photographs of each: (a) appearance of the alumina composite sheet using polydomain LCE, (b) appearance of wrapped and adhered to a 6 mm diameter aluminum pipe, and (c) a POM image of the alumina composite sheet under crossed Nicols (thickness= 300 μm).

Table 2. Thermal Conductivities and Elastic Modulus for LCE Alumina Composite Sheets and Reference Nonmesogenic Multifunctional Acrylic Elastomer Composite Sheets (Thickness= 300 μm)

composite material	75 vol % of alumina of LCE		75 vol % of alumina of Reference	
direction	∥ (in plane)	⊥ (out of plane)	∥ (in plane)	⊥ (out of plane)
thermal conductivity of composite [W/(m·K)]	16.5 ± 2.5	9.8 ± 0.6	8.5 ± 0.5	3.9 ± 0.2
density [g/cm3]	3.24 ± 0.05		3.20 ± 0.05	
specific heat capacity [J/(g·K)]	0.87 ± 0.03		0.88 ± 0.02	
elastic modulus [MPa]	70 ± 1		30 ± 1	

MPa, as shown in Table 2. The POM observation result indicates that different particle sizes of the alumina particles were evenly dispersed throughout the composite LCE material. Achieving good dispersibility is crucial as it greatly influences both thermal conductivity and insulation properties.[2] Table 2 shows the measurement results of thermal conductivities and the elastic modulus, where the orientation of the thermal conductivity measurements is indicated by ∥ for in-plane and ⊥ for out-of-plane (thickness) directions. For comparison, the thermal conductivity of the acrylic elastomer composite without mesogen is also provided in Table 2.

The LCE alumina composite sheet exhibits an average value of 9.8 W/(m·K) in the thickness direction. This value is over twice as high as that of the acrylic elastomer composite sheet without mesogen. Using Bruggeman's equation,[2,54−58] the thermal conductivity of the base resin was estimated to be 0.5 W/(m·K) from Figure 10. The apparent thermal conductivity of the LCE in the composite (0.50 W/(m·K)) being larger than that of the resin-only sheet (0.35 W/(m·K) in Table 1) is assumed to be due to the interfacial interaction and molecular orientation of the LCE molecules at the alumina interface in the composite.

4. CONCLUSIONS

In this paper, higher ordered structures were analyzed for the cross-linking acrylic liquid crystal elastomer (LCE), which exhibits transparency and flexibility while possessing high thermal conductivity in the in-plane direction. This transparent

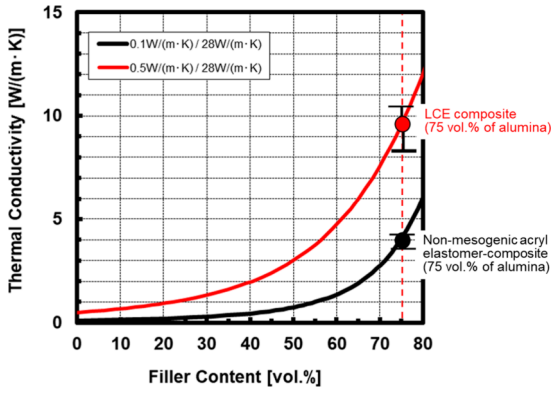

Figure 10. Composite thermal conductivity prediction and validation based on Bruggeman's equation.

monodomain LCE sheet was obtained by photocuring while stretching the polydomain LCE to 80% elongation. The thermal conductivity of the stretching direction (x) of this monodomain LCE sheet was 1.8 times higher, measuring 1.79 W/(m·K), compared to that of the prestretched polydomain sheet. Furthermore, regarding the thermal conductivity of the orthogonal direction (y) to the x-direction, which was measured at 3.0 W/(m·K), it was around 1.7 times higher than that of the x-direction.

From the XRD analysis, for the out-of-plane direction, the molecules in the monodomain LCE sheet were aligned in the

https://doi.org/10.1021/acsomega.3c09550
ACS Omega 2024, 9, 20839−20848

stretching *x*-direction. In contrast, for the in-plane direction, the molecular plane spacing was randomly oriented to the *x*-direction (i.e., heat transfer direction). However, in contrast, the molecular plane spacing was horizontally uniaxially oriented, exhibiting a highly ordered structure in the *y*-direction. Therefore, we conclude that the heat energy entering into the *y*-direction once spreads to the *x*-direction due to the higher ordered structure; subsequently, the synergistic effect of the covalent bonding structure due to photo-cross-linking in the *y*-direction contributes to its higher thermal conductivity compared to the *x*-direction.

Next, using the polydomain LCE, composite sheets filled with 75 vol % of alumina particles were fabricated and characterized. The alumina composite sheet exhibited high thermal conductivity along the thickness direction, averaging 9.8 W/(m·K), coupled with flexibility characterized by an elastic modulus of around 70 MPa. The thermal conductivity was over twice the value of 3.9 W/(m·K), which is measured in a nonmesogenic acrylic composite sheet with the same alumina particle filling. The apparent thermal conductivity of the base LCE resin in the composite was estimated to be 0.5 W/(m·K) using Bruggeman's composite's thermal conductivity prediction equation. These flexible composite sheets are expected to be applicable as thermal interface materials (TIM) in semiconductor applications and other related fields.

■ ASSOCIATED CONTENT

Supporting Information

The Supporting Information is available free of charge at https://pubs.acs.org/doi/10.1021/acsomega.3c09550.

> Preparation of LCE composite sheets, thermal diffusivity measurement system (ai-Phase mobile M3 type1), transmittance properties for two types of LCE sheets, higher-order structural analysis for polydomain and monodomain sheets using transmission 2D-WAXS, effect of thickness on XRD 2D-transmit WAXS for inner layer of sheets, and compared with 2D-transmit WAXS image of mesogenic epoxy thin sheet (PDF)

■ AUTHOR INFORMATION

Corresponding Author

Yoshitaka Takezawa − *Institute for Advanced Integrated Technology, Resonac Corporation, Tsukuba, Ibaraki 300-4247, Japan*; orcid.org/0009-0007-9278-2175; Email: takezawa.yoshitaka.xigpt@resonac.com

Authors

Naoki Furukawa − *Institute for Advanced Integrated Technology, Resonac Corporation, Tsukuba, Ibaraki 300-4247, Japan*

Senguttuvan Nachimuthu − *Institute for Advanced Integrated Technology, Resonac Corporation, Tsukuba, Ibaraki 300-4247, Japan*

Risheng Zhou − *Impressio, Inc., Denver, Colorado 80229, United States*

Amir Torbati − *Impressio, Inc., Denver, Colorado 80229, United States*

Complete contact information is available at: https://pubs.acs.org/10.1021/acsomega.3c09550

Notes

The authors declare no competing financial interest.

■ ACKNOWLEDGMENTS

We are grateful to Mr. Yusuke Ohori of the Open Facility Center, Ibaraki University, for his cooperation in the 2D-GI-WAXS & SAXS measurements and analysis using Rigaku SmartLab. We also thank Dr. Rajib Shaha and Dr. Christopher Yakacki for their contribution to this study.

■ REFERENCES

(1) Moore, A.; Shi, L. Emerging challenges and materials for thermal management of electronics. *Mater. Today* **2014**, *17*, 163−74.

(2) Chen, H.; Ginzburg, V. V.; Yang, J.; Yang, Y.; Liu, W.; Huang, Y.; Du, L.; Chen, B. Thermal conductivity of polymer-based composites: Fundamentals and applications. *Prog. Polym. Sci.* **2016**, *59*, 41−85.

(3) Ma, T.; Zhao, Y.; Ruan, K.; Liu, X.; Zhang, J.; Guo, Y.; Yang, X.; Kong, J.; Gu, J. Highly Thermal Conductivities, Excellent Mechanical Robustness and Flexibility, and Outstanding Thermal Stabilities of Aramid Nanofiber Composite Papers with Nacre Mimetic Layered Structures. *ACS Appl. Mater. Interfaces* **2020**, *12*, 1677−1686.

(4) Ruan, K.; Guo, Y.; Gu, J. Liquid Crystalline Polyimide Films with High Intrinsic Thermal Conductivities and Robust Toughness. *Macromolecules* **2021**, *54*, 4934−4944.

(5) Kittel, C. *Introduction to Solid State Physics*, Sixth ed; John Wiley & Sons, 1986

(6) Hansen, D.; Bernier, G. A. Thermal conductivity of polyethylene: The effects of crystal size, density and orientation on the thermal conductivity. *Polym. Eng. Sci.* **1972**, *12*, 204−208.

(7) Choy, C. L.; Luk, W. H.; Chen, F. C. Thermal conductivity of highly oriented polyethylene. *Polymer* **1978**, *19*, 155−162.

(8) Kanamoto, T.; Tsuruta, A.; Tanaka, K.; Takeda, M.; Porter, R. Super-drawing of ultrahigh molecular-weight polyethylene. 1. Effect of techniques on drawing of single-crystal mats. *Macromolecules* **1988**, *21*, 470−7.

(9) Piraux, L.; Kinanyalaoui, M.; Issi, J.; Begin, D.; Billaud, D. Thermal conductivity of an oriented polyacetylene film. *Solid State Commun.* **1989**, *70*, 427−9.

(10) Algaer, E. A.; Alaghemandi, M.; Böhm, M. C.; Müller-Plathe, F. Anisotropy of the thermal conductivity of stretched amorphous polystyrene in supercritical carbon dioxide studied by reverse non-equilibrium molecular dynamics simulations. *J. Phys. Chem. B* **2009**, *113*, 14596−603.

(11) Langer, L.; Billaud, D.; Issi, J. Thermal conductivity of stretched and annealed poly(p-phenylene sulfide) films. *Solid State Commun.* **2003**, *126*, 353−7.

(12) Osada, K.; Koike, M.; Tagawa, H.; Hunaoka, S.; Tokita, M.; Watanabe, J. Two distinct types of orientation process observed in uniaxially elongated smectic LC melt. *Macromolecules* **2005**, *38*, 7337−7342.

(13) Zhong, Z.; Wingert, M.; Strzalka, J.; Wang, H.; Sun, T.; Wang, J.; Chen, R.; Jiang, Z. Structure-induced enhancement of thermal conductivities in electrospun polymer nanofibers. *Nanoscale* **2014**, *6*, 8283−91.

(14) Zhang, X.; Wang, Y.; Xia, R.; Wu, B.; Chen, P.; Qian, J.; Liang, H. Effect of Chain Configuration on Thermal Conductivity of Polyethylene: A Molecular Dynamic Simulation Study. *Chin. J. Polym. Sci.* **2020**, *38*, 1418−1425.

(15) Shen, S.; Henry, A.; Tong, J.; Zheng, R.; Chen, G. Polyethylene nanofibres with very high thermal conductivities. *Nat. Nanotechnol.* **2010**, *5*, 251−255.

(16) Xu, Y.; Kraemer, D.; Song, B.; Jiang, Z.; Zhou, J.; Loomis, J.; Wang, J.; Li, M.; Ghasemi, H.; Huang, X.; Li, X.; Chen, G. Nanostructured polymer films with metal-like thermal conductivity. *Nat. Commun.* **2019**, *10*, 1771.

(17) Hammerschmidt, A.; Geibel, K.; Strohmer, F. In situ photopolymerized, oriented liquid-crystalline diacrylates with high thermal conductivities. *Adv. Mater.* **1993**, *5*, 107−109.

(18) Akatsuka, M.; Takezawa, Y. High Thermal Conductive Epoxy Resins Containing Controlled High Order Structures. *J. Appl. Polym. Sci.* **2003**, *89*, 2464−2467.
(19) Harada, M.; Ochi, M.; Tobita, M.; Kimura, T.; Ishigaki, T.; Shimoyama, N.; Aoki, H. Thermal-conductivity properties of liquid-crystalline epoxy resin cured under a magnetic field. *J. Polym. Sci., Part B: Polym. Phys.* **2003**, *41*, 1739−1743.
(20) Fukushima, K.; Takahashi, H.; Takezawa, Y.; Kawahira, T.; Itoh, M.; Kanai, J. High Thermal Conductive Resin Composites with Controlled Nanostructures for Electric Devices. *IEEJ. transactions on fundamentals and materials Transactions of IEE Japan* **2006**, *126*, 1167−1172.
(21) Song, S.; Katagi, H.; Takezawa, Y. Study on high thermal conductivity of mesogenic epoxy resin with spherulite structure. *Polymer* **2012**, *53*, 4489−4492.
(22) Koda, T.; Toyoshima, T.; Komatsu, T.; Takezawa, Y.; Nishioka, A.; Miyata, K. Ordering simulation of high thermal conductivity epoxy resins. *Polymer J.* **2013**, *45*, 444−448.
(23) Kim, D. G.; Kim, Y. H.; Shin, T. J.; Cha, E. J.; Kim, D. S.; Kim, B. G.; Yoo, Y.; Kim, Y. S.; Yi, M. H.; Won, J. C. Highly anisotropic thermal conductivity of discotic nematic liquid crystalline films with homeotropic alignment. *Chem. Commun.* **2017**, *53*, 8227−8230.
(24) Tanase, T.; Kato, T.; Tanaka, S.; Sano, A.; Kojima, H.; Fukushima, K.; Takezawa, Y. Prolonging Electrical Lifetime of Mesogenic Epoxy Based Alumina-Mica Composite Sheet: Optimization of Mica Content by Electrical Tree Progress Simulation. *IEEE Trans. on Dielectrics and Electrical Insulation* **2018**, *25*, 2212−2219.
(25) Tanaka, S.; Hojo, F.; Takezawa, Y.; Kanie, K.; Muramatsu, A. Formation of Liquid Crystalline Order and Its Effect on Thermal Conductivity of AlN/Liquid Crystalline Epoxy Composite. *Polym.-Plast. Technol. Eng.* **2018**, *57*, 269−275.
(26) Tanaka, S.; Hojo, F.; Takezawa, Y.; Kanie, K.; Muramatsu, A. Highly oriented liquid crystalline epoxy film: Robust high thermal conductive ability. *ACS Omega* **2018**, *3*, 3562−3570.
(27) Kang, D.-G.; Ko, H.; Koo, J.; Lim, S.-I.; Kim, J. S.; Yu, Y.-T.; Lee, C.-R.; Kim, N.; Jeong, K.-U. Anisotropic Thermal Interface Materials: Directional Heat Transfer in Uniaxially Oriented Liquid Crystal Networks. *ACS Appl. Mater. Interfaces* **2018**, *10*, 35557−35562.
(28) Tanaka, S.; Takezawa, Y.; Kanie, K.; Muramatsu, A. Homeotropically aligned monodomain-like smectic-A structure in liquid crystalline epoxy films: Analysis of the local ordering structure by microbeam small-angle Xray scattering. *ACS Omega* **2020**, *5*, 20792−20799.
(29) SUGII, T.; ITO, H.; MATSUMOTO, S.; TANAKA, S.; MORIYA, H.; MARUYAMA, N.; HOSHINO, M.; TANAKA, N.; TAKEZAWA, Y. Layer structure formation of mesogenic liquid crystalline epoxy resin during curing reactions: A reactive coarse-grained molecular dynamics study. *Mech. Eng. J.* **2021**, *8*, 20-00328−14.
(30) Ota, S.; Harada, M. Filler Surface Adsorption of Mesogenic Epoxy for LC Epoxy/MgO Composites with High Thermal Conductivity. *Composites: Part C* **2021**, *4*, No. 100087.
(31) Hasegawa, M.; Suyama, N.; Shimoyama, N.; Aoki, H.; Nunokawa, T.; Kimura, T. Enhanced thermal conductivity of semi-aliphatic liquid crystalline polybenzoxazoles using magnetic orientation. *Polym. Int.* **2011**, *60*, 1240−7.
(32) Yoshihara, S.; Ezaki, T.; Nakamura, M.; Watanabe, J.; Matsumoto, K. Enhanced thermal conductivity of thermoplastics by lamellar crystal alignment of polymer matrices. *Macromol. Chem. Phys.* **2012**, *213*, 2213−9.
(33) Harada, M.; Hamaura, N.; Ochi, M.; Agari, Y. Thermal conductivity of liquid crystalline epoxy/BN filler composites having ordered network structure. *Composites B* **2013**, *55*, 306−13.
(34) Yoon, D.; Lee, H.; Kim, T.; Song, Y.; Lee, T.; Lee, J.; Hun Seol, J. Enhancing the thermal conductivity of amorphous polyimide by molecular-scale manipulation. *Eur. Polym. J.* **2023**, *184*, No. 111775.
(35) Yang, X.; Zhong, X.; Zhang, J.; Gu, J. Intrinsic high thermal conductive liquid crystal epoxy film simultaneously combining with excellent intrinsic self-healing performance. *J. of Mater. Sci. & Technol.* **2021**, *68*, 209−215.
(36) Jeong, I.; Kim, C.; Kang, D.; Jeong, K.; Jang, S.; You, N.; Ahn, S.; Lee, D.; Goh, M. Liquid crystalline epoxy resin with improved thermal conductivity by intermolecular dipole−dipole interactions. *J. Polym. Sci., Part A: Polym. Chem.* **2019**, *57*, 708−715.
(37) Yang, X.; Zhu, J.; Yang, D.; Zhang, J.; Guo, Y.; Zhong, X.; Kong, J.; Gu, J. High efficiency improvement of thermal conductivities for epoxy composites from synthesized liquid crystal epoxy followed by doping BN fillers. *Composites Part B: Engineering* **2020**, *185*, No. 107784.
(38) Yorifuji, D.; Ando, S. Molecular Structure Dependence of Out-of-Plane Thermal Diffusivities in Polyimide Films: A Key Parameter for Estimating Thermal Conductivity of Polymers. *Macromolecules* **2010**, *43*, 7583−7593.
(39) Tang, N.; Tanaka, S.; Takezawa, Y.; Kanie, K. Highly anisotropic thermal conductivity of mesogenic epoxy resin film through orientation control. *J. Appl. Polym. Sci.* **2021**, *138*, 51396.
(40) Shimazaki, Y.; Miyazaki, Y.; Takezawa, Y.; Nogi, M.; Abe, K.; Ifuku, S.; Yano, H. Excellent Thermal Conductivity of Transparent Cellulose Nanofiber/Epoxy Resin Nanocomposites. *Biomacromolecules* **2007**, *8*, 2976−2978.
(41) Kang, D. G.; Park, M.; Kim, D. Y.; Goh, M.; Kim, N.; Jeong, K. U. Heat Transfer Organic Materials: Robust Polymer Films with the Outstanding Thermal Conductivity Fabricated by the Photopolymerization of Uniaxially Oriented Reactive Discogens. *ACS Appl. Mater. Interfaces* **2016**, *8*, 30492−30501.
(42) Saed, M. O.; Torbati, A. H.; Starr, C. A.; Visvanathan, R.; Clark, N. A.; Yakacki, C. M. Thiol-Acrylate Main-Chain Liquid-Crystalline Elastomers with Tunable Thermomechanical Properties and Actuation Strain. *J. Polym. Sci., PART B: Polym. Phys.* **2017**, *55*, 157−168.
(43) Saed, M. O.; Torbati, A. H.; Nair, D. P.; Yakacki, C. M. Synthesis of Programmable Main-chain Liquid-crystalline Elastomers Using a Two-stage Thiol-acrylate Reaction. *JoVE* **2016**, *107*, No. e53546.
(44) Torbati, A. H.; Mather, P. T. A hydrogel-forming liquid crystalline elastomer exhibiting soft shape memory. *J. Polym. Sci., Part B: Polym. Phys.* **2016**, *54*, 38−52.
(45) Kato, H.; Baba, T.; Okaji, M. Anisotropic thermal-diffusivity measurements by a new laser-spot-heating techniqu. *Meas. Sci. Technol.* **2001**, *12*, 2074−2080.
(46) Hashimoto, T.; Matsui, Y.; Hagihara, A.; Miyamoto, A. Thermal diffusivity measurement of polymer films by the temperature wave method using joule-heating. *Thermochim. Acta* **1990**, *163*, 317.
(47) Hashimoto, T.; Tsuji, T. Thermal diffusivity measurement of polyethylene melt by a new temperature wave method. *J. Therm. Anal.* **1993**, *40*, 721−726.
(48) Tanaka, K.; Ogata, S.; Kobayashi, R.; Tamura, T.; Kouno, T. A molecular dynamics study on thermal conductivity of thin epoxy polymer sandwiched between alumina fillers in heat-dissipation composite material. *Int. J. Heat Mass Transfer* **2015**, *89*, 714−723.
(49) Ogata, S.; Uranagase, M.; Takahashi, Y.; Kishi, T. First Principles Calculations of the Protonation and Weakening of Epoxy Resin under Wet Conditions. *Journal of Physical Chemistry. B* **2021**, *125*, 8989−8996.
(50) Ju, Y. S.; Kurabayashi, K.; Goodson, K. E. Thermal characterization of anisotropic thin dielectric films using harmonic Joule heating. *Thin Solid Films* **1999**, *339*, 160−164.
(51) Nasir, A.; Rahman, M. Cybotactic nematic liquid crystal: an overview. *Liquid Crystals.* **2024**, 1 DOI: 10.1080/02678292.2024.2313003.
(52) Saha, S.; Mohiuddin, G.; Paul, M.; Gupta, S.; Khan, R.; Ghosh, S.; Pal, S. Polar Switching and Cybotactic Nematic Ordering in 1,3,4-Thiadiazole-Based Short-Core Hockey Stick-Shaped Fluorescent Liquid Crystals. *ACS Omega* **2019**, *4*, 7711−7722.
(53) Kaur, S.; Mohiuddin, G.; Zhang, J.; Chakraborty, S.; Ding, X.; Verma, D.; Sinha, A.; Xiang, Y.; Pal, S. Polar response and

https://doi.org/10.1021/acsomega.3c09550
ACS Omega 2024, 9, 20839−20848

Fréedericksz transition in cybotactic nematic fluids of unsymmetrical bent-core molecules. *J. Mol. Liq.* **2023**, *387*, No. 122626.
(54) Bruggeman, D. A. G. Berechnung Verschiedener Physikalischer Kon-stanten von Heterogenen Substanzen, I. Dielektrizitatskonstan-tenund Leitfahigkeiten der Mischkorper aus Isotropen Substanzen. *Annal Phys. Leipz.* **1935**, *24*, 636−79.
(55) Agari, Y.; Ueda, A.; Nagai, S. Thermal conductivity of a polymer composite. *J. Appl. Polym. Sci.* **1993**, *49*, 1625−34.
(56) Sanada, K.; Tada, Y.; Shindo, Y. Thermal conductivity of polymercomposites with close-packed structure of nano and micro fillers. *Composites A* **2009**, *40*, 724−30.
(57) Chen, J.; Wei, H.; Bao, H.; Jiang, P.; Huang, X. Millefeuille Inspired Thermally Conductive Polymer Nanocomposites with Overlapping BN Nanosheets for Thermal Management Applications. *ACS Appl. Mater. Interfaces* **2019**, *11*, 31402−31410.
(58) Zhang, R.; Shi, X.; Tang, L.; Liu, Z.; Zhang, J.; Guo, Y.; Gu, J. Thermally Conductive and Insulating Epoxy Composites by Synchronously Incorporating Si-sol Functionalized Glass Fibers and Boron Nitride Fillers. *Chin. J. Polym. Sci.* **2020**, *38*, 730−739.

https://doi.org/10.1021/acsomega.3c09550
ACS Omega 2024, 9, 20839−20848